

APR-2 TROPICAL CYCLONE OBSERVATIONS

S. L. Durden and S. Tanelli
Jet Propulsion Laboratory, California Institute of Technology

1. INTRODUCTION

The Second Generation Airborne Precipitation Radar (APR-2) participated in the Genesis and Rapid Intensification Processes (GRIP) experiment in August and September of 2010, collecting a large volume of data in several tropical systems, including Hurricanes Earl and Karl. Additional measurements of tropical cyclone have been made by APR-2 in experiments prior to GRIP (namely, CAMEX-4, NAMMA, TC4); Table 1 lists all the APR-2 tropical cyclone observations.

The APR-2 observations consist of the vertical structure of rain reflectivity at 13.4 and 35.6 GHz, and at both co-polarization and cross-polarization, as well as vertical Doppler measurements and crosswind measurements. APR-2 normally flies on the NASA DC-8 aircraft, as in GRIP, collecting data with a downward-looking, cross-track scanning geometry. The scan limits are 25 degrees on either side of the aircraft, resulting in a roughly 10-km swath, depending on the aircraft altitude. Details of the APR-2 observation geometry and performance can be found in Sadowy et al. (2003).

The multiparameter nature of the APR-2 measurements makes the collection of tropical cyclone measurements valuable for detailed studies of the processes, microphysics and dynamics of tropical cyclones, as well as weaker systems that are associated with tropical cyclone formation. In this paper, we give a brief overview of how the APR-2 data are processed. We also discuss use of the APR-2 cross-track winds to estimate various quantities of interest in studies of storm intensification. Finally, we show examples of the standard products and derived information.

2. APR-2 DATA PROCESSING

The standard APR-2 data processing first requires that the radar data be synchronized with the aircraft navigation data. For GRIP both the standard aircraft data and higher-quality GPS data were collected. The navigation data are used to estimate the aircraft orientation, providing a Doppler correction for the data. This correction is also estimated from the radar surface return's Doppler (Durdan et al. 1999). Generally, the two

Table 1. APR-2 tropical cyclone observations

Date	Tropical Cyclone
8/20/01	TS Chantal
9/15	TS Gabrielle
9/22	TS Humberto
9/23	H Humberto
9/24	H Humberto
8/23/06	TS Debby
9/12	Depression Helene
8/29/10	H Earl
8/30	H Earl
9/1	H Earl
9/2	H Earl
9/14	TS Karl
9/16	H Karl
9/17	H Karl

approaches compare quite well, and the surface Doppler is normally used, but the navigation-estimated correction is also provided in the standard data product.

The radar data are initially calibrated using data recorded through a calibration loop in the radar. Final calibration is based on the ocean backscatter at 10 degrees for Ku-band. At this incidence angle, the surface return is least sensitive to wind speed. The Ka-band calibration is then adjusted to agree with the Ku-band measurements in very light precipitation, based on Mie scattering calculations. The APR-2 calibration is described in more detail in Tanelli et al. (2006).

APR-2 records both the co-polarized and cross-polarized return at both frequencies. From these measurements we estimate the linear depolarization ratio (LDR). By using the Doppler measurements over a scan and assuming horizontal uniformity at each altitude, we can solve for the vertical and horizontal velocity components at each altitude. For reasonably well-organized tropical cyclones, we were typically flying radial tracks, so the cross-track wind serves as an estimate of the cyclone's azimuthal wind. In reality, the radial may not be exact, and the aircraft is likely yawed, so the cross-track direction deviates from the azimuthal direction relative to storm center.

3. ADDITIONAL QUANTITIES OF INTEREST

In this section we discuss several quantities that can be derived from the standard products. We can infer the location of melting ice

Corresponding author address: 4800 Oak Grove Dr., Pasadena, CA 91109; email: sdurden@jpl.nasa.gov.

from the LDR parameter noted above. We can also form the difference of the Ku-band and Ka-band reflectivities. In ice, one expects low attenuation and small difference between the two reflectivities if the ice particles are small. However, as the particles increase in size, they leave the Rayleigh scattering regime at Ka-band. Their reflectivity decreases relative to Ku-band, so ZKu-ZKa (in dB) can reach several dB. This dual-wavelength ratio (DWR) is used to identify areas with larger ice particle sizes.

The inertial frequency in a vortex is the usual Coriolis frequency f_o modified by the vortex. It is:

$$f^2 = \left(f_o + \frac{2v}{r} \right) \left(f_o + \frac{v}{r} + \frac{\partial v}{\partial r} \right) \quad (1)$$

where v is the azimuthal velocity. As the inertial frequency increases, the vortex stiffens, making it easier for energy from latent heating to go into the transverse circulation, rather than going into oscillations and being radiated away. Specifically, one can examine the Rossby length (Vigh and Schubert 2009), which is the internal gravity wave speed divided by f . The Rossby length is the length beyond which rotational effects become as important as buoyancy effects. Another quantity related to f is the Ekman layer thickness, defined as the square root of twice the eddy viscosity divided by f .

Also of interest is the warm-core structure of the storm. While radar isn't sensitive to density or thermal structure, such structure can be inferred by assuming a vortex in gradient and hydrostatic balance. Smith (2006) derives a method to estimate the pressure, density, and temperature structure under such assumptions, given the azimuthal wind field, as a function of radius and altitude. To do so, he derives a thermal wind equation and then uses the anelastic approximation:

$$\frac{\partial p}{\partial r} = \rho_o \left(\frac{v^2}{r} + fv \right) \quad (2)$$

$$\frac{\partial \rho}{\partial r} = -\frac{1}{g} \frac{\partial}{\partial z} \left[\rho_o \left(\frac{v^2}{r} + fv \right) \right]$$

In these equations, p is pressure, r is density, ρ_o is environmental density, g is gravitational acceleration, f is the Coriolis parameter, and v is the azimuthal velocity. The surface pressure is 1013 hPa and the surface density is 1.2 kg/m^3 . A constant lapse rate of 6.5 K/km is used for the environmental temperature profile. We use a finite difference approximation and then integrate

at each altitude to get pressure and density versus radius. Then temperature is derived using the ideal gas law.

4. HURRICANE EARL

This section examines the APR-2 standard products and derived quantities for Hurricanes Earl and Karl of 2010.

4.1 Hurricane Earl

Earl became a tropical storm on 8/25 when it was located to the west of the Cape Verde Islands. It continued across the Atlantic at tropical storm strength, followed by a period of rapid intensification, reaching Category 1 on the Saffir-Simpson scale on 8/29 and Category 4 on the 30th. Its Intensity fluctuated over the next two days, dropping to Category 3 and then reaching its maximum intensity on 9/1. As it moved to higher latitudes, it was impacted by southerly shear and weakened. APR-2 data were acquired on 8/29, 8/30, 9/1, and 9/2. Here we concentrate on the rapid Intensification period of 8/29 and 8/30.

Figure 1 shows the Ku-band reflectivity, Ku-band LDR, Ka-band reflectivity, and the DWR for 8/29. Although the eye was not particularly distinct visually (at least from the DC-8 altitude), it does appear in the APR-2 data at 20:29:52 UTC. The flight track was east to west, and the stronger convection appears to the east of the eye (left side of the image). On this side, the strongest convection is adjacent to the eye. Peak reflectivity is at least 45 dBZ, and strong attenuation can be seen at Ka-band in several locations; white areas just above the surface indicate poor SNR due to attenuation.

Figure 2 shows the corresponding wind data. The yellow and red areas at upper levels just to the left of the eye indicate fairly strong updrafts ($>10 \text{ m/s}$). The XWIND image (azimuthal velocity) shows several maxima; it can be argued that the strongest convection is inside the radius of maximum wind. According to Vigh and Schubert (2009), this allows the heating from the convection to better contribute to the storm's secondary circulation and intensification. Calculations of the Rossby length indicate that it decreases from an environmental value of more than 1000 km to a roughly 100 km near the center. This indicates that the heating at the center is located in a vortex that is stiffening. We also computed this same quantity from flight level wind measurements from an Air Force reconnaissance flight and found a similar result. Also shown in Figure 2 is the pressure deficit derived from Smith's method (2a). The maximum pressure deficit in the eyewall is around 35 hPa, fairly consistent with a minimal hurricane. The central pressure was near 975 hPa, as measured by aircraft dropsonde.

Figure 3 shows the CFAD for ZKu (i.e., reflectivity histogram at each altitude) in the inner

core region, along with CFADs for the vertical and azimuthal velocities. The CFAD for azimuthal velocity is bimodal, since velocities on the right side of the storm are opposite (negative) those on the left (positive).

Figures 4-6 show the same quantities as in Figure 1-3 but for August 30. The retrieved pressure deficit 65 hPa, consistent with a dropsonde measured MSLP of 950 hPa. The reflectivity and velocity statistics are fairly similar to that for 8/29, although the maximum azimuthal wind speed is, of course, considerably larger, with winds on the left side exceeding 50 m/s. As a result of the stronger wind field, the minimum Rossby length is reduced to around 50 km. For both days we found that the Ekman layer depth is over 1000 m at the edge of the storm and reduces to several hundred m near the storm center, similar to the observations of Zhang et al. (2011). Due to the stronger winds, the Ekman layer is thinner on 8/30.

4.2 Hurricane Karl

Karl also formed from a disturbance that originated in the eastern Atlantic. However, its path was south of Earl's, entering the eastern Caribbean Sea as a disturbance and finally becoming a depression and tropical storm on 9/14. Figure 11 shows the Ku-band reflectivity and velocity data from 9/14. The crosswind image shows the circulation with center determined by the change in winds from positive to negative. At the time of the APR-2 data acquisition, the area did not have intense convection; the reflectivity appears to show mostly stratiform rainfall.

ACKNOWLEDGEMENT

This study was carried out at the Jet Propulsion Laboratory, California Institute of Technology, under a contract with the National Aeronautics and Space Administration.

REFERENCES

- Durden, S. L., Z. S. Haddad, and T. P. Bui, 1999: Correction of Doppler radar data for aircraft motion using surface measurements and recursive least-squares estimation," *J. Atmos. Oceanic Technol.*, **16**, 2026-2029.
- Heymsfield, A. J., A. Bansemer, S. L. Durden, R. L. Herman, and T. P. Bui, 2009: Ice microphysics observations in Hurricane Humberto: Comparison with non-hurricane-generated ice cloud layers. *J. Atmos. Sci.*, **63**, 288-308.
- Sadowy, G. A., A. C. Berkun, W. Chun, E. Im, and S. L. Durden, 2003: Development of an advanced airborne precipitation radar. *Microwave J.*, **46**, 84-98.
- Schubert, W. H., and B. D. McNoldy, 2010: Application of the concepts of Rossby length and Rossby depth to tropical cyclone dynamics. *J. Adv. Model Earth Syst.*, **2**, 7.
- Smith, R. K., 2006: Accurate determination of a balanced axisymmetric vortex in a compressible atmosphere. *Tellus*, **58A**, 98-103.
- Tanelli, S., S. L. Durden, and E. Im, 2006: Simultaneous Measurements of Ku- and Ka-band Sea Surface Cross-Sections by an Airborne Radar. *IEEE Geosci. Remote Sens. Lett.*, **3**, 359-363.
- Vigh, J. L., and W. H. Schubert, 2009: Rapid development of the tropical cyclone warm core. *J. Atmos. Sci.*, **66**, 3335-3350.
- Zhang, J. A., R. F. Rogers, D. S. Nolan, and F. D. Marks, 2011: On the characteristic height scales of the hurricane boundary layer. *Mon Wea. Rev.*, **139**, 2524-2535.

© 2011 California Institute of Technology.
Government sponsorship acknowledged.

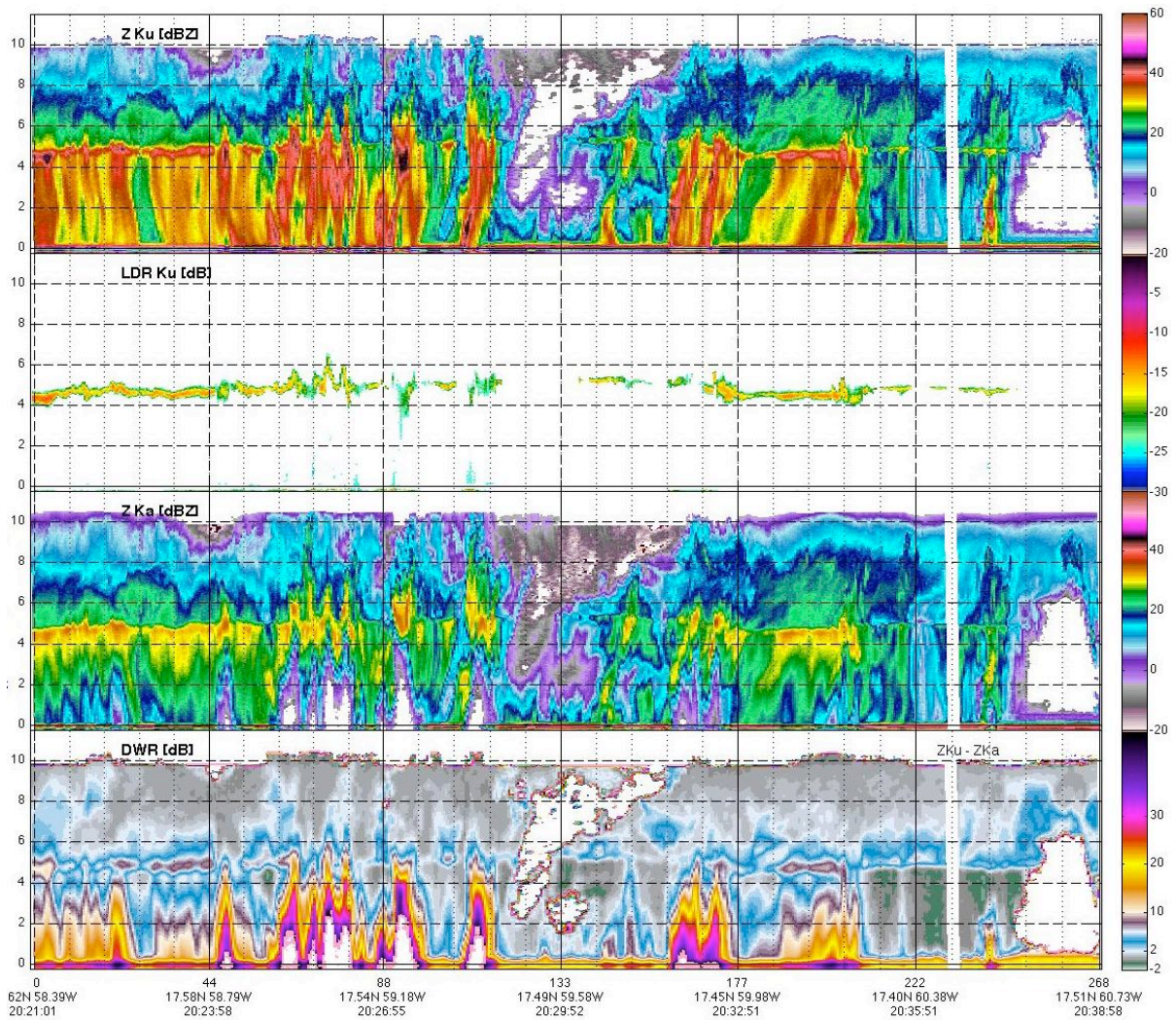


Figure 1. APR-2 measurements of Hurricane Earl on August 29, 2010.

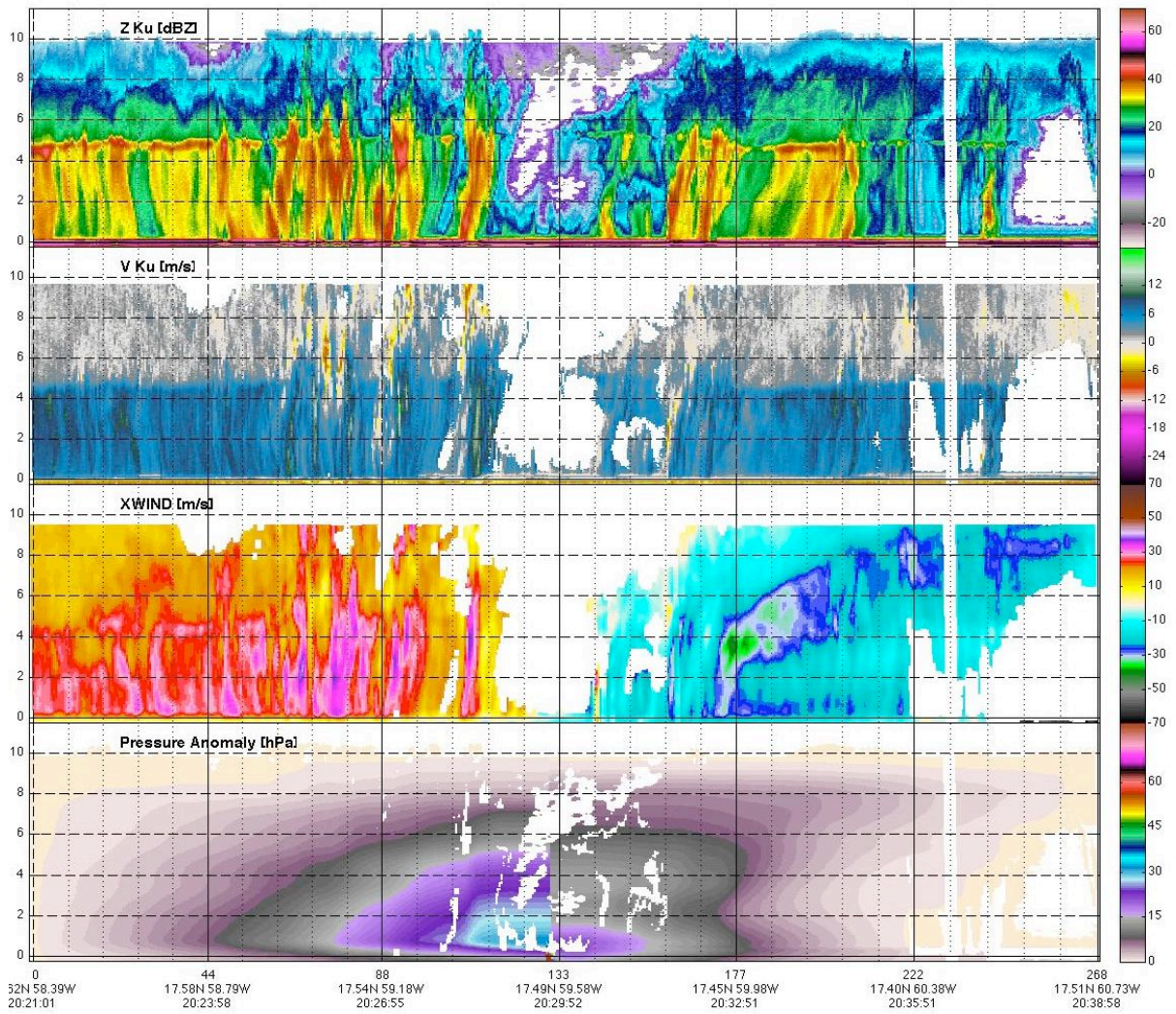


Figure 2. APR-2 measurements of Hurricane Earl on August 29, 2010

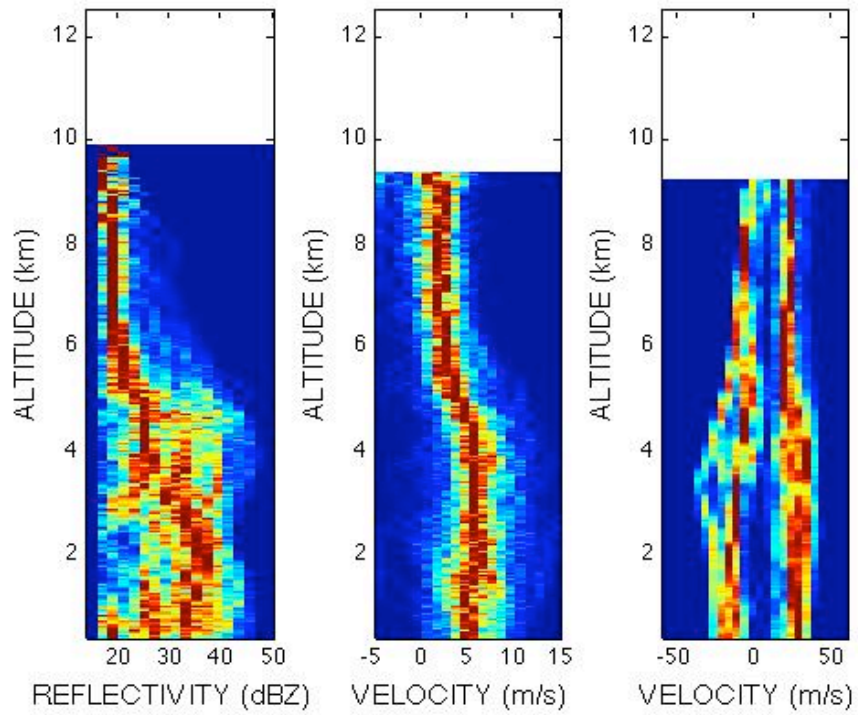


Figure 3. CFADs for reflectivity (left), vertical velocity (middle), and azimuthal velocity (right) for Hurricane Earl on August 29, 2010.

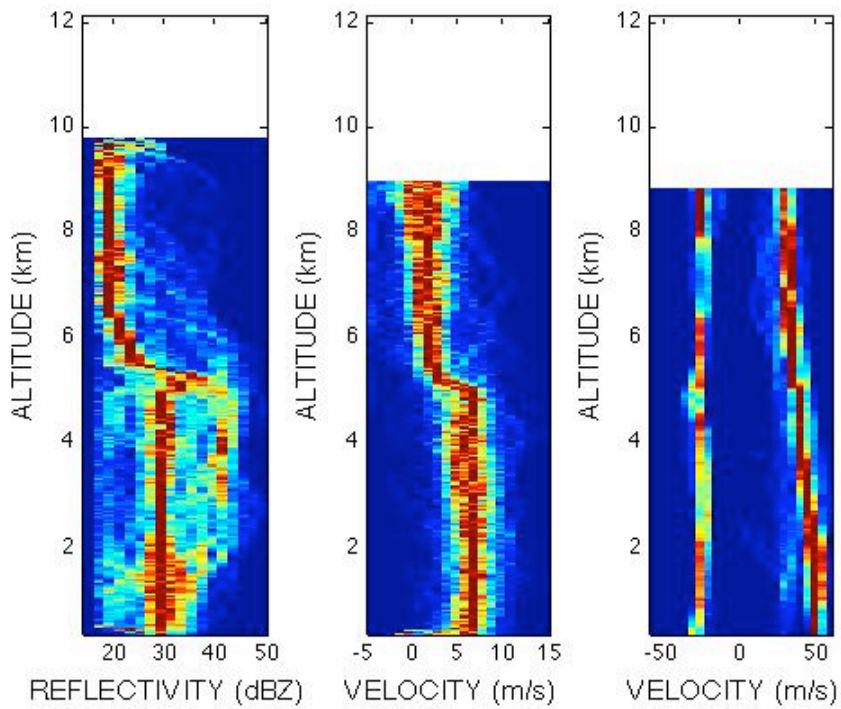


Figure 4. CFADs for reflectivity (left), vertical velocity (middle), and azimuthal velocity (right) for Hurricane Earl on August 30, 2010.

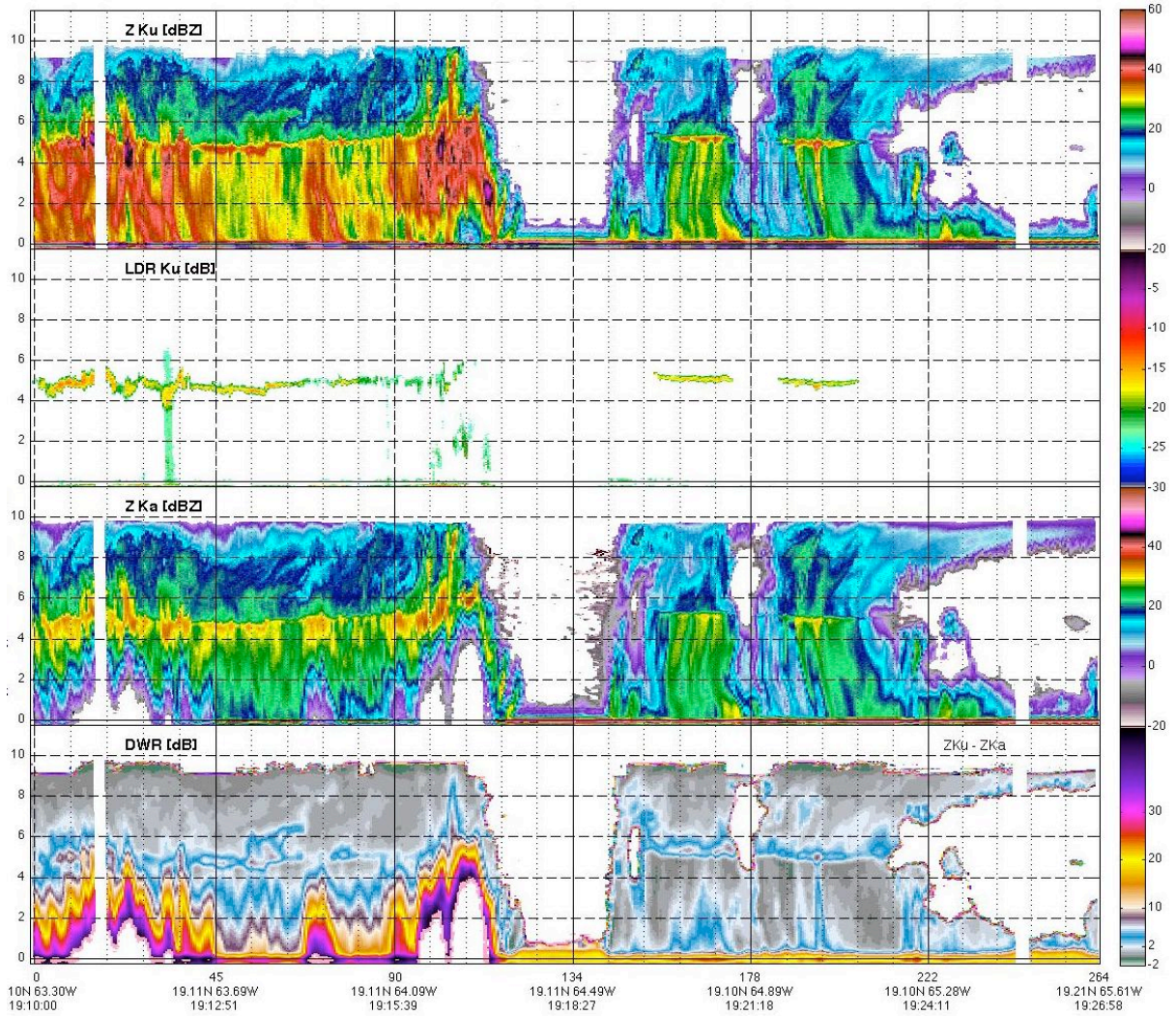


Figure 5. APR-2 measurements of Hurricane Earl on August 30, 2010

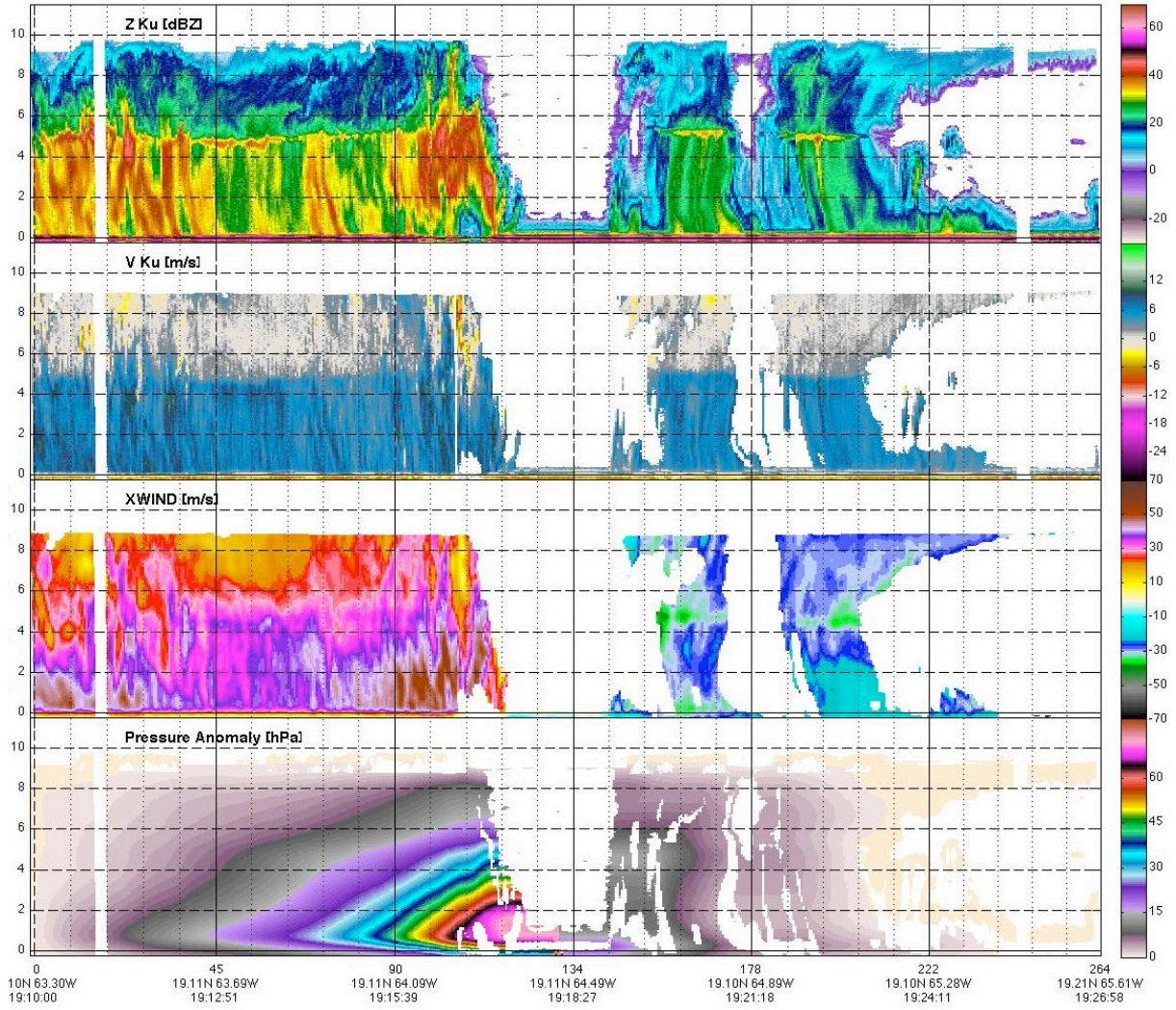


Figure 6. APR-2 measurements of Hurricane Earl on August 30, 2010